Proc. Natl. Acad. Sci. USA
Vol. 94, pp. 5427–5431, May 1997
Neurobiology

Voltage-controlled gating in a large conductance Ca^{2+}-sensitive K^+channel (hslo)

E. STEFANI†‡§, M. OTTOLIA†¶, F. NOCETI†, R. OLCESE†, M. WALLNER†, R. LATORRE†‖, AND L. TORO†§**

Departments of †Anesthesiology and ‡Physiology, and the §Brain Research Institute, University of California, Los Angeles, CA 90095; ‖Centro de Estudios Cientificos de Santiago, Casilla 16443, and Departamento de Biologia, Facultad de Ciencias, Universidad de Chile, Santiago, 9 Chile

Communicated by Lily Yeh Jan, University of California School of Medicine, San Francisco, CA, March 11, 1997 (received for review October 3, 1996)

ABSTRACT **Large conductance calcium- and voltage-sensitive K^+ (MaxiK) channels share properties of voltage- and ligand-gated ion channels. In voltage-gated channels, membrane depolarization promotes the displacement of charged residues contained in the voltage sensor (S4 region) inducing gating currents and pore opening. In MaxiK channels, both voltage and micromolar internal Ca^{2+} favor pore opening. We demonstrate the presence of voltage sensor rearrangements with voltage (gating currents) whose movement and associated pore opening is triggered by voltage and facilitated by micromolar internal Ca^{2+} concentration. In contrast to other voltage-gated channels, in MaxiK channels there is charge movement at potentials where the pore is open and the total charge per channel is 4–5 elementary charges.**

Large conductance voltage- and Ca^{2+}-sensitive potassium channels (MaxiK or K_{Ca}) are important modulators of neuronal firing and vascular tone (1–3). Their open probability raises when the cytoplasmic calcium concentration increases or when the plasma membrane is depolarized. MaxiK channels seemed to require the presence of calcium to open (i.e., calcium gated) (4–6) and to lack an intrinsic voltage sensor (7). However, indirect evidence using chemical modifications suggested that MaxiK channels can open in response to voltage without the requirement of intracellular calcium (8). Consistent with these results, we demonstrated that depolarization can open MaxiK channels (hslo) in a calcium-independent manner (9). This indicates that MaxiK channels have a purely voltage-dependent mode of gating and demands the existence of a voltage sensor. Indeed, MaxiK channels possess a transmembrane domain (S4 region) (10, 11) analogous to the one that, in other voltage-gated K channels, has been proposed to be the voltage sensor (12–15). The movement of this voltage sensor, triggered by depolarization, can be directly measured as gating currents (16–18). We show that MaxiK channels possess an intrinsic voltage sensor able to induce measurable voltage-dependent gating currents. As previously shown for ionic currents (9), these gating currents are purely voltage-dependent at low internal Ca^{2+} concentration ($[Ca^{2+}]_i$); however, a raise in $[Ca^{2+}]_i$ to micromolar levels diminishes the voltage necessary to move a given amount of charge. These results strongly suggest that in MaxiK channels, micromolar Ca^{2+} functions as a "facilitator" by diminishing the electrical work needed to activate the voltage-gating machinery.

MATERIALS AND METHODS

Clones and Expression Systems Used. hslo (GenBank accession no. U11058) cDNAs starting from the third (*hsloM3*), or fourth (*hsloM4*) (19) Kozak consensus sequence for translational initiation were used. High level expression was obtained by subcloning hslo into a vector carrying at the 5′ end a 183-bp untranslated region of ShakerH4 K^+ channel and at the 3′ end a stretch of 30 thymidine residues. *Xenopus laevis* oocytes were injected with 45 nl of cRNA at 0.2 μg/μl and kept at 18°C for 4–7 days. Gating currents were also recorded in HEK cells transfected with *hsloM3* subcloned in pCDNA3 vector (Invitrogen). HEK cells expressing the large T antigen protein of SV40 virus were cotransfected with *hsloM3* and the α subunit of the human CD8 lymphocyte surface antigen. Before recording, cells were labeled with anti-CD8-coated beads (Dynal, Great Neck, NY) to select for transfected cells (20). Shaker H4-IR in pBluescript (Stratagene) was expressed in *Xenopus laevis* oocytes (21).

Solutions. Bath and pipette solutions contained 110 mM methanesulfonate·*X* (*X*-MES), 10 mM Hepes, and 0.1 mM ouabain (22) at pH 7 where *X* was potassium, *N*-methylglucamine, tetraethylammonium (TEA), or cesium. Pipette solutions contained 2 mM $CaCl_2$. Solutions with different $[Ca^{2+}]_i$ were prepared with 5 mM HEDTA, *N*-(2-Hydroxyethyl)ethylenediaminetriacetic acid and $CaCl_2$ according to Chelator (23), taking into account 9 μM contaminant Ca^{2+} in buffer-free solutions as measured with a Ca^{2+} electrode. Free Ca^{2+} was then checked with a Ca^{2+} electrode (micromolar range; World Precision Instruments, Sarasota, FL) or with Fura-2 (nanomolar range).

Electrical Recordings. Cs^+ currents were recorded after equilibrating the intracellular space with Cs^+; to accelerate this process, oocytes were mechanically perforated. To measure gating currents in the same oocytes, we used external TEA. We have compared gating currents with and without TEA at voltages near channel opening. Under these conditions gating currents were not modified by the presence of TEA. However, it is not established whether at higher potentials, external TEA could affect charge movement. Pulse duration was 20–25 ms for ionic and 1–20 ms for gating currents; short 1-ms pulses were used for better time resolution and to avoid membrane breakdown due to extreme positive and negative potentials. One-millisecond pulses were adequate to evaluate hslo charge movement (quasi steady state), since its main component has a time constant of decay of $\approx$60 μs, indicating that the majority of the charge moves in the first millisecond. However, a slow component in the charge movement becomes apparent as the duration of the voltage pulse increases from 1 to 10 ms. This slow component amounts to a maximum of 15%

Abbreviations: MaxiK (or hslo), large conductance calcium- and voltage-sensitive K^+; $[Ca^{2+}]_i$, internal calcium concentration; MES, methanesulfonate; TEA, tetraethylammonium; *Q-V*, charge to voltage relationship; *G-V*, conductance to voltage relationship; SHP, subtracting holding potential; TP, test pulse; HP, holding potential.

¶Present address: Istituto di Cibernetica e Biofisica, Consiglio Nazionale delle Ricerche, Genova, Italy.
**To whom reprint requests should be addressed at: Department of Anesthesiology, BH-612 CHS, Box 951778, University of California, Los Angeles, CA 90095-1778. e-mail: ligia@cvmail.anes.ucla.edu.

The publication costs of this article were defrayed in part by page charge payment. This article must therefore be hereby marked "*advertisement*" in accordance with 18 U.S.C. §1734 solely to indicate this fact.

0027-8424/97/945427-5$2.00/0
PNAS is available online at **http://www.pnas.org**.

of the total charge at the midpoint of the charge to voltage relationship (Q–V) curve and induces a leftward shift of about 20 mV. The Q–V curves obtained with 10 and 20 ms pulses are essentially the same. Since the slow component is a small fraction of the total charge, Q–V curves cross the conductance to voltage relationship (G–V) curves with either 1-ms or 20-ms voltage pulses. Thus, 1-ms pulses were adequate to construct quasi steady-state Q–V curves. Q–V and G–V curves (Figs. 2 and 3) were analyzed in the same oocyte to eliminate large variations seen from oocyte to oocyte in K^+ (19) or in Cs^+ solutions. In Cs^+ solutions, the SD of the midpoints of G-V curves in cell-attached patches was ±25 mV ($V_{1/2}$ = 151 ± 25 mV, n = 15) and in 10 μM Ca^{2+}, the SD was ±10 mV ($V_{1/2}$ = 52 ± 10, n = 10). Midpoints of Q–V curves also vary among oocytes [$V_{1/2}$ in the cell-attached mode was 190 ± 15 mV (n = 19) in nine oocytes].

Acquisition Parameters. Gating and linear capacitive currents were usually acquired at 8 μs per point and filtered at 10 kHz. Ionic currents were usually acquired at 100 μs per point. We selected subtracting holding potentials (SHPs) by first checking the absence of gating currents at those potentials (cell-attached mode, SHP ≤ 0 mV; 85 μM Ca^{2+}, SHP ≤ −100 mV).

Conductance Ratios. Conductance ratios g_K/g_{Cs} were calculated with g_K of 290 pS (single channel conductance in symmetrical 110 mM K^+) (19) and g_{Cs} from variance analysis (24) (see also Fig. 4). Variance analysis of 128–256 consecutive current traces from −100 mV to membrane potential (V_m) = 100–130 mV, in inside-out patches (10 μM and 85 μM Ca^{2+}), was used to obtain unitary Cs^+ current (i_{Cs}). g_{Cs} was then calculated from $g_{Cs} = [i_{Cs}/(V_m - V_{Cs})]$, where V_{Cs} = 0 mV. i_{Cs} was independent of $[Ca^{2+}]_i$ and was 70 ± 12 fA (n = 5) at 100 mV. Mean g_{Cs} = 0.72 ± 0.1 pS (n = 7).

Number of Charges per Channel. To evaluate the number of charges per channel, we measured in the same oocyte, in different but adjacent areas, the limiting charge movement (Q_{max}) using TEA-MES (pipette) and the number of channels (N) with nonstationary variance analysis (24) (see Fig. 4) using Cs-MES (pipette). To estimate the patches surface, we measured the membrane capacity (C_m) of each patch, which allowed us to calculate Q_{max} and N per unit surface. The main assumption for this measurement is that channels are homogeneously distributed in the oocyte membrane. Channel clustering or inhomogeneities in channel distribution were minimized because we used large patch pipettes; we consistently obtained similar density values for channels in individual oocytes. After measuring the C_m in each patch [using 2 ms pulses to 10 mV from holding potential (HP) = 0 mV], pulse protocols were given to measure gating currents to obtain Q_{max} or to measure ionic current noise to estimate N. Q_{max} and N were then normalized by their corresponding C_m to obtain Q_{max}* (Q_{max}/surface) and N* (N/surface). Number of charges per channel = Q_{max}*/e^-N*, where e^- is the elementary charge (1.6×10^{-19} coulombs).

Statistics. Values are means ± SD. Student's t test was used; results were considered significantly different at $P \leq 0.001$.

RESULTS AND DISCUSSION

Hslo Gating Currents Precede Ionic Currents. Gating currents from hslo could be successfully recorded after maximizing the level of expression and by using large patch pipettes (15–25 μm). In Fig. 1, we show representative examples of hslo gating and ionic currents measured in cell-attached patches using either isotonic Cs^+ (Fig. 1 *B* and *C*) or K^+ (Fig. 1*D*). Because gating currents are much smaller than ionic currents, the measurement of both ionic and gating currents in patches of the same oocyte (Figs. 1 *B* and *C*, and 2–4), required the use of a permeant ion with small unitary conductance, Cs^+. Human MaxiK channels (hslo) are permeable to Cs^+ similar

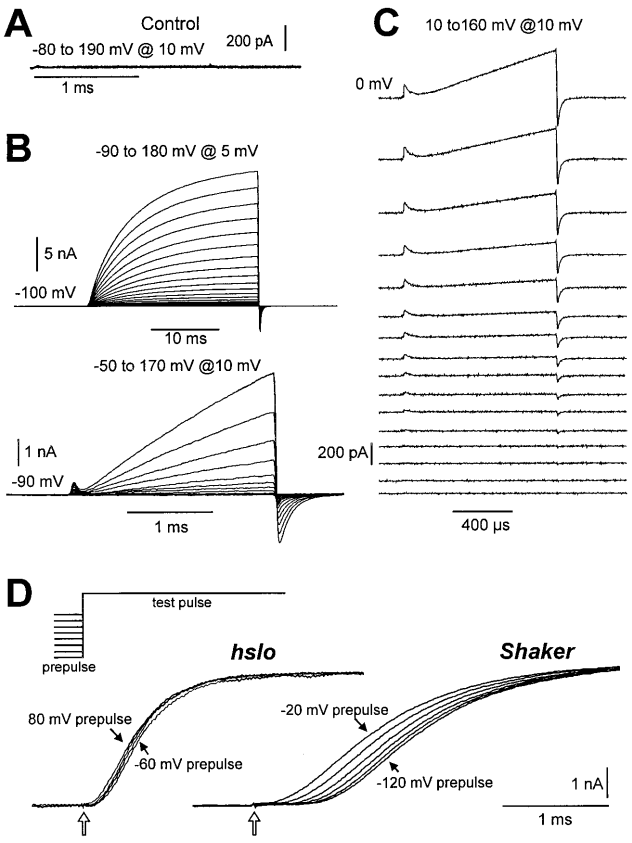

FIG. 1. MaxiK (hslo) gating currents. (*A*) Uninjected oocyte. HP = −90 mV. In this and the following figures, numbers at the top of traces indicate the test pulses (TP). P/-4, SHP = −90 mV (Pl-4, negative pulses of 1/4 test-pulse amplitude from subtracting holding potential (SHP) used to obtain scaled control currents to digitally subtract linear capacity and resistive components). K-MES solution. (*B*) Cs^+ and gating currents. Cs-Mes solution. Top traces: HP = 0 mV, 10 ms/−100 mV–TP–100 ms/−100 mV (prepulse–TP–postpulse). Lower traces: HP = 0 mV, 800 μs/−90 mV–TP–50 ms/−90 mV. P/4, SHP = −120 mV. (*C*) High-resolution recordings. Acquired at 0.5 μs per point; filtered at 200 kHz. Amplifier, acquisition system, and software were custom made. HP = 0 mV. SHP = −50 mV, P/-2. Traces are average of 100 runs. Cs-MES solution. (*D*) Cole–Moore effect in hslo (to the left) and in Shaker H4 K^+ (to the right) channels. Hslo currents in an HEK-transfected cell. (*Inset*) Pulse protocol (not to scale). HP = −100 mV. Traces correspond to 400-μs prepulses to −60, 40, 60, and 80 mV, followed by a constant TP = 150 mV. Pipette and bath solution were 140 mM K-MES, 10 mM glucose, 10 mM Hepes, 2 mM $MgCl_2$, pH 7 and pCa 5. Shaker H4 K^+ (inactivation removed, Δ6–46 deletion) currents in oocytes (21). HP = −100 mV. Traces belong to 800-μs prepulses (400 μs is illustrated) to −120 mV to −20 mV every 20 mV followed by a constant TP = 50 mV. Bath solution was 110 mM K-MES, 2 mM $MgCl_2$, 0.1 mM EGTA, 10 mM Hepes, pH 7.0. Pipette solution was 110 mM K-MES, 2 mM $CaCl_2$, 10 mM Hepes, pH 7.0. Open arrows mark the onset of the test pulse. (*A–D*) Cell-attached mode.

to Shaker K channels; their conductance ratio g_K/g_{Cs} is about 400 (405 ± 58, n = 7; g_{Cs} = 0.72 ± 0.1 pS, n = 7; g_k = 290 ps) (19), which is 4-fold larger than that of Shaker K channels (25). Thus, the use of Cs^+ allowed the recording of otherwise unmeasurable huge ionic currents together with gating currents. This type of gating and ionic currents were absent in oocytes not injected with hslo cRNA (Fig. 1*A*). High-resolution records in Fig. 1*C* (acquired at 0.5 μs per point) show that gating currents predominantly precede the ionic current at low activation potentials and that with larger depolarizations, after the initial component of the gating current, the onset of ionic currents overlaps the decay of gating currents. The fact that gating currents precede channel open-

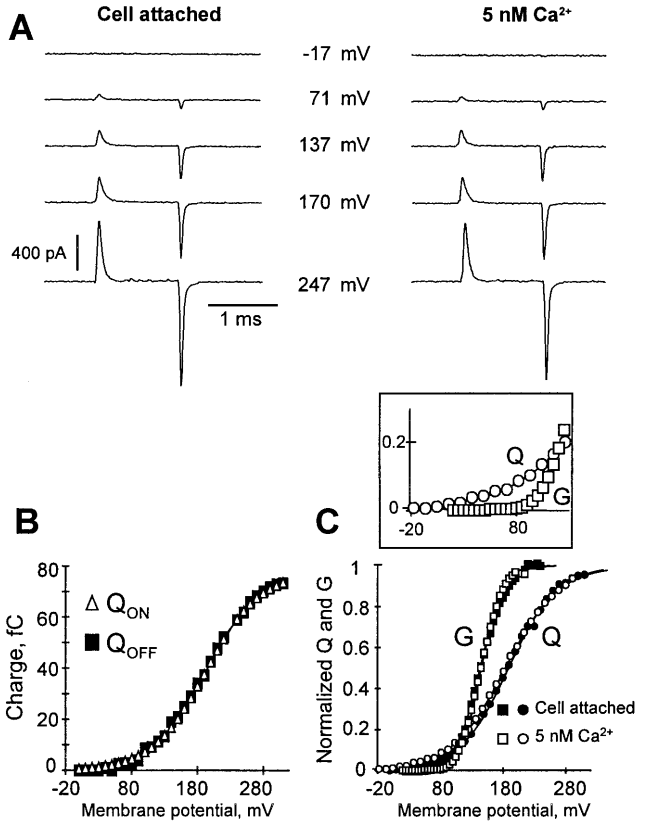

FIG. 2. Properties of MaxiK gating currents and Ca independence. (*A*) Gating currents in cell-attached (≈100 nM Ca^{2+}) and in 5 nM Ca^{2+} (inside-out) in the same patch. HP = 0 mV. 800 μs/−90 mV–TP–50 ms/−90 mV. TPs are indicated. P/4, SHP = −90 mV. (*B*) ON and OFF charge are equal ($Q_{ON} = Q_{OFF}$). Charge values (Q) were obtained by integrating gating currents during (ON) and after the pulse (OFF). (*C*) Normalized voltage-activation curves for gating currents (Q) (currents in *A*) and ionic currents (G) in cell-attached mode and in 5 nM $[Ca^{2+}]_i$ from the same oocyte. (*Inset*) Expanded region. Q_{OFF} was measured. Conductance (G) values were obtained according to $G = I_{Cs}/(V_m - V_{Cs})$, where I_{Cs} is the macroscopic Cs^+ current, V_m is the membrane potential, and V_{Cs} is reversal potential for Cs^+ (0 mV). I_{Cs} was measured from tail currents as the amplitude of a single exponential fit from records similar to those shown in Fig. 1*B*. For description purposes, data points were fitted to Boltzmann distributions: $X = X_{max}/\{1 + \exp[(V_{1/2} - V_m)zF/RT]\}$, where X may be Q or G, other terms have their usual meaning. Fitted values were, for cell-attached, $V_{1/2-G}$ = 147 mV, z_G = 1.3, and $V_{1/2-Q}$ = 192 mV, z_Q = 0.6; and for 5 nM Ca^{2+}, $V_{1/2-G}$ = 144 mV, z_G = 1.6 and $V_{1/2-Q}$ = 184 mV, z_Q = 0.6. Solutions were as follows: bath, Cs-MES; pipette, for gating currents, TEA-MES, for ionic currents (G—V curves), Cs-MES.

ing suggests the presence of more than one closed state through which the channel transits before it opens. Consistent with this view, the onset of the hslo K^+ current elicited during a depolarization can be delayed by hyperpolarizing prepulses (Fig. 1*D*). The hyperpolarizing prepulses bring the channel to deeper closed states (Cole–Moore shift) (26) delaying its opening. The Cole–Moore shift observed in hslo, however, is less voltage-dependent than the one present in Shaker K channels (21) (Fig. 1*D*). This shallower voltage dependency of the current delay in hslo may be explained by a smaller proportion of the total charge carried by the transitions that precede channel opening (e.g., Fig. 2*C*).

Characteristics of Gating Currents and the Number of Charges per Channel in hslo. Gating currents from hslo were isolated from ionic currents by blocking the latter with external TEA (cell-attached or inside-out) or by substituting K^+ for the nonconducting ion *N*-methylglucamine (inside-out). The size of the gating currents was proportional to the level of functional expression as measured from the ionic current. The general characteristics of hslo gating currents recorded with external TEA (Figs. 2 and 3) or with *N*-methylglucamine are similar: (*i*) they are fast transient currents with a decay time constant at the ON (of a voltage step) of 57 ± 10 μs (n = 11, cell-attached, 200 mV) and (*ii*) the amount of charge moved at the ON (Q_{ON}) is equal to the charge measured at the end of the pulse (Q_{OFF}) (Fig. 2*B*). The number of charges per channel was 4.4 ± 0.8 (n = 3 cells). This value was obtained by normalizing both the number of channels (estimated from variance analysis) (24), and the limiting charge (Q_{max}) per membrane capacity individually measured in three to six giant patches of the same cell. This number is smaller than the one obtained for other voltage-gated ion channels of the S4 superfamily (27, 28). In Shaker K channel, the first four positive charges in S4 (29, 30) and a negative charge in S2 (glutamate-293) (30) contribute to a gating charge of about 13 charges per channel. Comparing S2 and S4 regions of hslo and Shaker K channels (11, 31), hslo lacks one of the four critical positive charges in S4 and the negative charge in S2. In a simplistic way, our results are consistent with the view that less charges in these critical S2 and S4 regions result in less gating charges per channel. Given the differences in the gating properties of hslo and Shaker K channels reported in this work, it will be interesting to study the functional role of these or other residues in hslo.

Gating Charge Moves Between Open States. Coupling between charge movement and pore opening of MaxiK channels was analyzed constructing voltage-activation curves of both gating (Q–V) and ionic (G–V) currents. A comparison of the properties of the two types of curves is meaningful only if gating and ionic current measurements are performed in the same oocyte (Figs. 2 and 3). This is due to the fact that G–V curves of MaxiK channels measured in different oocytes vary in their midpoint by about ±20 mV, when recorded at constant $[Ca^{2+}]_i$ in either K^+ (19) or Cs^+.

The most striking and unique feature in the coupling between charge movement and pore opening of MaxiK channels is that for small depolarizations the Q–V curve is negative to the G–V curve (Fig. 2*C Inset*) but crosses it near its foot leading to a Q–V curve positive to the G–V curve for larger depolarized potentials (e.g., Fig. 2*C*). This result suggests that upon depolarization little charge movement is needed to reach the initial open state(s) of the channel, in agreement with the small Cole–Moore shift (Fig. 1*D*), and that open-to-open transitions can carry charge. However, to explain the fast decay of the gating current with respect to the slow rising phase of the ionic current, it is necessary to postulate the existence of distant open to open transitions that are voltage-independent or that carry a very small amount of charge. The fact that charge can move along transitions between open states in MaxiK channels is in marked contrast with other voltage-gated ion channels, where most of the charge moves before pore opening (practically no charge moves in the last close to open transition), giving Q–V curves negative to G–V curves (32, 33).

Limiting Gating Charge and Limiting Open Probability Are Independent of $[Ca^{2+}]_i$. We have recently reported that at "resting" internal Ca^{2+} (as in the cell-attached patches) or below (≤100 nM) depolarization can induce hslo ionic currents in a Ca^{2+}-independent manner. Half-activation potentials are indistinguishable in the intact cell (cell-attached) at 100 nM, 10 nM, or 3 pM $[Ca^{2+}]_i$ (9), suggesting that hslo has a Ca^{2+}-independent way of gating. In agreement with these findings, gating currents measured in the same patch in cell-attached mode (≈100 nM Ca^{2+}) were indistinguishable from gating currents measured in the presence of 5 nM Ca^{2+} after excision (Fig. 2*A*), as depicted by the superimposed voltage-activation curves (e.g., Fig. 2*C*). In three paired experiments, $V_{1/2}$ values were, in the cell-attached mode, 167 ±

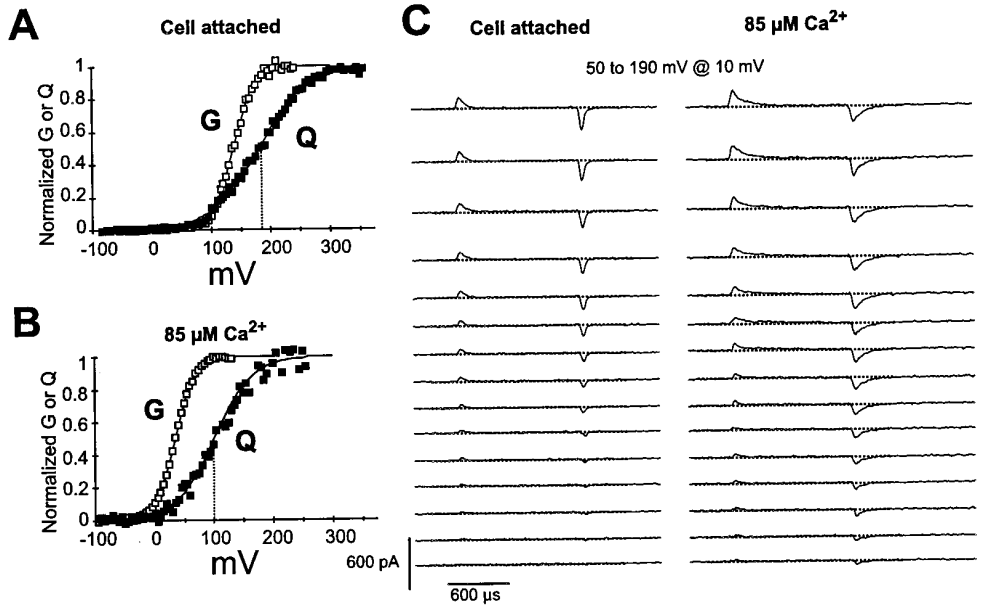

FIG. 3. Micromolar Ca^{2+} shifts *Q–V* and *G–V* curves. (*A* and *B*) Comparison of *Q–V* and *G–V* curves in the cell-attached mode and in 85 μM Ca^{2+} in the same cell. Data points were obtained and fitted as in Fig. 2. Dotted lines mark $V_{1/2}$ values for *Q–V* curves. Fitted values were as follows: for cell-attached, $V_{1/2-G}$ = 137 mV, z_G = 1.4; $V_{1/2-Q}$ = 180 mV, z_Q = 0.6; for 85 μM Ca^{2+}, $V_{1/2-G}$ = 35 mV, z_G = 1.5; $V_{1/2-Q}$ = 100 mV, z_Q = 0.7. (*C*) Corresponding gating current records in cell-attached mode (≈100 nM Ca^{2+}) and after excision of the same patch in 85 μM free Ca^{2+}. SHP = −120 mV. Solutions and pulse paradigms were as in Fig. 2.

18 mV and, in 5 nM Ca^{2+}, 172 ± 11 mV, which do not differ significantly. Thus, these results strongly suggest that hslo undergoes Ca^{2+}-independent closed–closed transitions that lead to Ca^{2+}-independent channel opening.

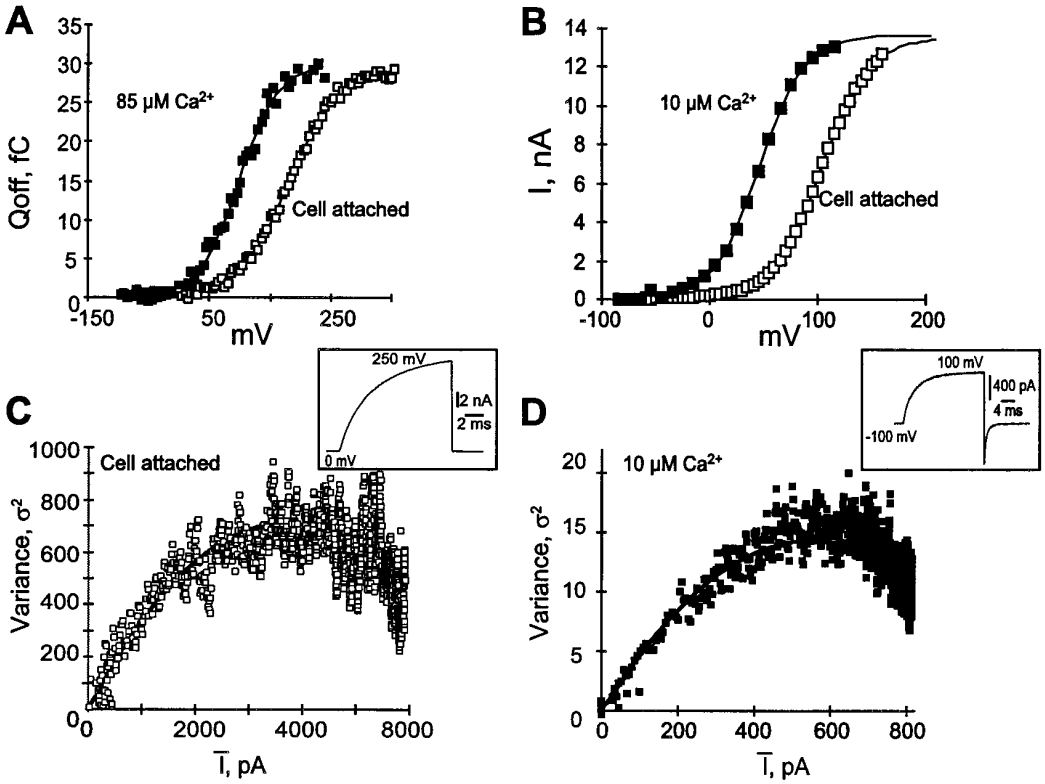

FIG. 4. Limiting amount of charge and maximum open probability are independent of $[Ca^{2+}]_i$. (*A*) Net charge vs. potential at two $[Ca^{2+}]$ in the same patch. (*B*) Cs^+ tail current (at −90 mV) vs. potential in cell-attached (≈100 nM Ca^{2+}) and after excision in 10 μM Ca^{2+}. (*C* and *D*) Nonstationary variance analysis (24). Values were fitted (continuous line) to $\sigma^2_{(t)} = \bar{I}_{(t)} - \bar{I}^2_{(t)}/N$. $\sigma^2_{(t)}$ = variance; $\bar{I}_{(t)}$ = mean current, i = unitary current; N = number of channels. Fitted values, calculated Po_{max} and g are as follows: for cell-attached (64 traces), Po_{max} = 0.8, i_{Cs} = 0.37 pS, g = 1.4 pS, N = 18,974; for 10 μM Ca^{2+} (256 traces) Po_{max} = 0.78, i_{Cs} = 0.058 pS, g = 0.77 pS, N = 2,487. The larger conductance value in the cell-attached mode for this experiment can be explained by an incomplete exchange of intracellular K^+ by Cs^+, which does not significantly affect Po_{max} ($Po_{max} = \bar{I}_{max}/iN$). (*Insets*) Cell-attached trace, HP = 0 mV and TP = 250 mV; 10 μM Ca^{2+} trace, HP = 0 mV, prepulse–TP–postpulse = 2 ms/−100 mV–TP–250 ms/−100 mV, and TP = 100 mV.

To understand the role of micromolar Ca^{2+} in the coupling between charge movement and pore opening, we investigated the effect of micromolar calcium on gating currents. *G–V* and *Q–V* curves shifted to more negative potentials after calcium was raised from "resting" (cell-attached; Fig. 3*A*) to micromolar calcium after excision (e.g., 85 μM in Fig. 3*B*). At 50 mV, practically no gating current was recorded in the cell-attached mode, whereas clear gating currents were recorded in 85 μM Ca^{2+} (Fig. 3*C*). In paired experiments, $V_{1/2}$ values of *Q–V* curves shifted from 192 ± 18 mV in cell-attached to 135 ± 16 mV in 10 μM Ca^{2+} ($n = 9$) and to 105 ± 17 mV in 85 μM Ca^{2+} ($n = 5$). It seems therefore that even though Ca^{2+} is not needed to trigger the gating machinery or to reach the open state(s) (Figs. 1 and 2), micromolar amounts of Ca^{2+} promote these processes by switching the channel conformation to a state where it requires less voltage to open the gate. Consistent with this idea, Fig. 4 shows that the amount of charge moved (Fig. 4*A*) and the maximum amount of current flow (fig. 4*B*) are the same regardless of the $[Ca^{2+}]_i$. The mean ratio of charge moved in the cell-attached mode to charge moved in micromolar Ca^{2+} was 0.9 ± 0.1 ($n = 10$). Since Ca^{2+} does not change either the single-channel amplitude (i) or the number of channels (N) in the patch, the experiment in Fig. 4*B* indicates that the maximum open probability is reached in both conditions, *Ca^{2+}*-independent (cell-attached) and *Ca^{2+}*-modulated (micromolar Ca^{2+}). To further corroborate this point, we measured noise fluctuations of ionic currents in cell-attached and in micromolar Ca^{2+} (Fig. 4 *C* and *D*). Maximum open probability was reached in both cases. Mean values were 0.78 ± 0.03 in cell-attached ($n = 6$), 0.76 ± 0.04 ($n = 4$) in 10 μM Ca^{2+} and 0.78 ± 0.03 in 100 μM Ca^{2+} ($n = 3$).

Our results suggest that MaxiK channels (hslo) can operate in two ways, a *Ca^{2+}*-independent mode and a *Ca^{2+}*-modulated mode, and that micromolar Ca^{2+} favors the switch to the *Ca^{2+}*-modulated mode. In each mode the kinetic and steady-state properties may be described with a model with several closed (C) states (at least 10) with voltage-dependent transitions. The last three closed states would be connected in parallel to open states (O) with relatively slow $C \rightleftharpoons O$ voltage-independent transitions. The relatively small Cole–Moore shift in hslo channel together with the crossing of the *Q–V* and *G–V* curves near their foot points that the charge carried along the initial $C \rightleftharpoons C$ transitions is a small percentage of the total charge. The fact that the *Q–V* curve comes positive to the *G–V* curve indicates the presence of charged transitions among open states, which is in agreement with the overlap of the decay of the gating currents with the onset of the ionic currents for large depolarizations. In the *Ca^{2+}*-modulated mode the equilibrium is shifted toward the open states. A modal type of gating for the *Ca^{2+}*-dependent mode has been recently proposed for the *Drosophila* MaxiK channel, where slow fluctuations in open probability with time were observed (34).

We conclude that MaxiK channels possess an intrinsic voltage sensor whose activation is obligatory to open hslo channels and that open transitions also carry charge. Thus, MaxiK channels are not Ca^{2+}-gated, as previously thought, but voltage-gated. Micromolar calcium transforms the channel from a *Ca^{2+}*-independent mode into a *Ca^{2+}*-modulated mode that requires less electrical energy to reach the open states.

The expression plasmid πH3-CD8 was kindly provided by Dr. Brian Seed (Massachusetts General Hospital, Boston). We thank Dr. F. Bezanilla for discussions and his participation in the development of the fast acquisition system. This work was supported by National Institutes of Health grants to L.T. (HL-54970) and E.S. (GM-52203) by Fondo Nacional de Investigacion (FNI 94-0227 and 97-739), and by Catedra Presidencial (Chile) to R.L. This work was done during the tenure of L.T. of an Established Investigatorship from the American Heart Association.

1. Crest, M. & Gola, M. (1993) *J. Physiol. (London)* **465,** 265–287.
2. Robitaille, R., Garcia, M. L., Kaczorowski, G. J. & Charlton, M. P. (1993) *Neuron* **11,** 645–655.
3. Nelson, M. T., Cheng, M. R., Santana, L. F., Bonev, A. D., Knot, H. J. & Lederer, W. J. (1995) *Science* **270,** 633–637.
4. Wong, B. S. & Lecar, H. (1982) *Biophys. J.* **39,** 313–317.
5. Moczydlowski, E. & Latorre, R. (1983) *J. Gen. Physiol.* **82,** 511–542.
6. McManus, O. B. & Magleby, K. L. (1991) *J. Physiol. (London)* **443,** 739–777.
7. Salomao, L., Wark, G., Dubinsky, W. P. & Schultz, S. G. (1992) *Am. J. Physiol.* **262,** C971–C974.
8. Pallotta, B. S. (1985) *J. Gen. Physiol.* **86,** 601–611.
9. Meera, P., Wallner, M. & Toro, L. (1996) *FEBS Lett.* **382,** 84–88.
10. Atkinson, N. S., Robertson, G. A. & Ganetzky, B. (1991) *Science* **253,** 551–555.
11. Adelman, J. P., Shen, K. Z., Kavanaugh, M. P., Warren, R. A., Wu, Y. N., Lagrutta, A., Bond, C. T. & North, R. A. (1992) *Neuron* **9,** 209–216.
12. Papazian, D. M., Timpe, L. C., Jan, Y. N. & Jan, L. Y. (1991) *Nature (London)* **349,** 305–310.
13. Perozo, E., Santacruz-Toloza, L., Stefani, E., Bezanilla, F. & Papazian, D. M. (1994) *Biophys. J.* **66,** 345–354.
14. Adrian, R. H. (1978) *Annu. Rev. Biophys.* **7,** 85–112.
15. Mannuzzu, L. M., Moronne, M. M. & Isacoff, E. Y. (1996) *Science* **271,** 213–216.
16. Armstrong, C. M. & Bezanilla, F. (1973) *Nature (London)* **242,** 459–461.
17. Schneider, M. F. & Chandler, W. K. (1973) *Nature (London)* **242,** 244–246.
18. Bezanilla, F., Perozo, E., Papazian, D. M. & Stefani, E. (1991) *Science* **254,** 679–683.
19. Wallner, M., Meera, P., Ottolia, M., Kaczorowski, G., Latorre, R., Garcia, M. L., Stefani, E. & Toro, L. (1995) *Recept. Channels* **3,** 185–199.
20. Jurman, M. E., Boland, L. M., Liu, Y. & Yellen, G. (1994) *BioTechniques* **17,** 876–881.
21. Stefani, E., Toro, L., Perozo, E. & Bezanilla, F. (1994) in *Handbook of Membrane Channels: Molecular and Cellular Physiology*, ed. Peracchia, C. (Academic, San Diego), pp. 29–40.
22. Rakowski, R. F. (1993) *J. Gen. Physiol.* **101,** 117–144.
23. Schoenmakers, T. J., Visser, G. J., Flik, G. & Theuvenet, A. P. (1992) *BioTechniques* **12,** 870–874, 876–879.
24. Sigworth, F. J. (1980) *J. Physiol. (London)* **307,** 131–142.
25. Heginbotham, L. & MacKinnon, R. (1993) *Biophys. J.* **65,** 2089–2096.
26. Cole, K. S. & Moore, J. W. (1960) *Biophys. J.* **1,** 161–202.
27. Schoppa, N. E., McCormack, K., Tanouye, M. A. & Sigworth, F. J. (1992) *Science* **255,** 1712–1715.
28. Noceti, F., Baldelli, P., Wei, X., Qin, N., Toro, L. & Birnbaumer, L. (1996) *J. Gen. Physiol* **108,** 143–155.
29. Aggarwal, S. K. & MacKinnon, R. (1996) *Neuron* **16,** 1169–1177.
30. Seoh, S. A., Sigg, D., Papazian, D. M. & Bezanilla, F. (1996) *Neuron* **16,** 1159–1167.
31. Wallner, M., Meera, P. & Toro, L. (1996) *Proc. Natl. Acad. Sci. USA* **93,** 14922–14927.
32. Stefani, E., Toro, L., Perozo, E. & Bezanilla, F. (1994) *Biophys. J.* **66,** 996–1010.
33. Neely, A., Wei, X., Olcese, R., Birnbaumer, L. & Stefani, E. (1993) *Science* **262,** 575–578.
34. Silberberg, S. D., Lagrutta, A., Adelman, J. P. & Magleby, K. L. (1996) *Biophys. J.* **70,** 2640–2651.